Calibration and field deployment of low-cost fluid flow-rate sensors using a wireless network

C. K. Harnett, M. T. Schueler, and N. R. Blumenthal
Electrical and Computer Engineering
University of Louisville
Louisville, KY 40292
c0harn01@gwise.louisville.edu

J. F. Fox and S. Pulugurtha
Civil Engineering
University of Kentucky
Lexington, KY 40506
jffox@engr.uky.edu

K. L. Hopf
Eastern Kentucky University
Richmond, KY 40475

***Abstract*—Low-cost networked fluid flow velocity sensors are needed for high-density sampling in environmental research and other applications requiring automated fluid flow velocity mapping. The flow sensor in this report is the "target" type consisting of a flap that deflects in the flow, changing the resistance of a strain gauge. A highly compliant flexible resistor promises to reduce costs by serving as the flow target and by eliminating signal amplification circuitry needed for conventional strain gauges. However, we show that individual calibration of these resistive sensors is critical for recovering the stream flow velocity. A wireless network is used for mass calibration of multiple sensors in a test flume. After individual sensor calibrations are obtained, the same wireless network can be used to collect flow velocity data in the sensor application. A modular connection system enables the user to quickly reconfigure the system's physical layout for calibration or deployment purposes. Results are reported on an outdoor deployment of the flow sensors for logging stream flow data in environmental research.**

Keywords-calibration, distributed measurement systems, environmental sensors, wireless sensor networks

I. INTRODUCTION

Fluid flow velocity sensors are needed for mapping stream flows in fundamental studies of erosion (the research area targeted by the sensors in this report), and in more applied areas such as closed-loop control in chemical processing. Because a high sensor spatial density is needed for mapping, and the sensors are generally deployed in harsh environments, a low-cost rugged transducer is desirable. An inexpensive flexible printed resistive element can work as a flow sensor, but since small differences in strain-vs-resistance characteristics translate into large differences in the flow velocity-vs-output voltage curve, individual calibration is needed to match the sensor's output voltage to a particular flow velocity in meters per second. Because the sensors are designed to interface with a wireless network, simultaneous calibration of multiple sensors is possible.

This report describes the construction of flow sensor circuits based on deflection of a flexible resistive element, the Flexpoint "Bend Sensor." The performance of these flow sensors is compared to that of a Sontek acoustic Doppler velocity sensor. A wireless sensor network is used for simultaneous calibration of multiple sensors in a test flume, producing individual calibration coefficients for storage in a database alongside the sensor's serial number. Finally, the sensor network is reconfigured for deployment and visualization of the flow velocity data.

The flow sensor here is one element of a multiparameter sensing system for aquatic environmental measurements described in previous work [1,2]. This article provides more detail on the flow sensor, and a new mass calibration method that takes advantage of the built-in sensor serial number and wireless network interface. In addition, new analysis and information is presented with regards to the velocity bend sensor that will aid in measuring mean velocity and velocity distributions, in space and time, for turbulent open channel flow in flumes and rivers. The new analysis encompasses the effect of fluid drag on sensor shape and sensor voltage, the variation of sensor output due to turbulent conditions and water temperature, field deployment in a turbulent stream, and discussion of future modifications needed for widespread use of the sensing system.

II. FLOW SENSOR SPECIFICATIONS

In this application, expected flow velocities range up to a few meters/s during storms, with typical flows at ~0.5 m/s or less. The flow is turbulent, with Reynolds numbers in the range of 10,000 and above when the Bend Sensor's 2-inch length is used as the characteristic length. A flow velocity uncertainty of 1.5 cm/s (~3% of the flow velocity) is acceptable, and a measurement rate of 1 sample per minute is adequate. The sensors need to be low-cost ($20 US) so they can be installed densely—in some cases, 20 cm apart to monitor the flow over a cross-section of a small stream near the origin of a watershed.

The devices will stay in the stream for approximately 3 weeks between maintenance visits, and their readings will

This work was supported by the National Science Foundation under Grant 0644511.

complement periodical point measurements from a higher-resolution ADV sensor. The temperature ranges from -20 C to 40C, and they are typically under at most 3 m of water (hydrostatic pressure ~ 30 kPa). Because power is supplied to multiple sensors by a 4-AA battery pack, the sensors need to consume on average <1 mW of power for the supply to last the entire 3 weeks. This is largely achieved by turning the sensors off between measurements. Finally, sensors need to be protected from debris and insensitive to fouling by algae.

Besides the environmental and cost requirements, the specifications include some usability requirements. The long-term goal is a system that can be installed by users without a measurement or engineering background (for instance, K-12 students), yet can upload reliable data for global environmental studies. It should be possible to deploy the system with minimal programming, hardware modification, and record-keeping, and the resulting data should be stored in a standard format compatible with online databases. Therefore, we include error-checking methods, timestamping, and automatic recognition of individual sensor spatial location and orientation in the specification list and discuss methods for accomplishing these aims.

III. Flow Sensor Design And Analysis

There are numerous established flow sensing methods including acoustic Doppler velocimetry (ADV) and rate-counting of a propeller immersed in the flow. ADV provides high-quality, high speed (50 Hz) data, but is relatively expensive. Electromagnetic flow sensors are insensitive to particles and bubbles, but are costly [3] and consume more power than a resistive sensor. Propellers are a low-cost alternative but are subject to fouling by algae, which could slow or stop their rotation. A bendable element is expected to be less sensitive to fouling. The flow sensor in this report consists of a voltage divider with a fixed (10 kOhm) resistor and a variable resistor (the Bend Sensor) with a resistance that increases from ~4 kOhm to ~20 kOhm when deflected. We found that of the varieties of available BendSensors, the two-inch polyimide-coated type had a good dynamic range over the typical flow velocities expected in the environmental sensor application. For basic performance testing, we used a wired data acquisition system to monitor the analog signal at the output of the voltage divider, while for mass calibration and deployment, the voltage divider was interfaced to a 16-bit A/D converter (DS2450) that also provides multidrop addressability over a 1-Wire interface, and assigns a unique serial number to each sensor. A complete flow sensor with waterproof housing is shown in Fig. 1 alongside its voltage divider circuit.

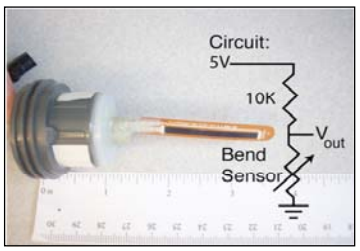

Fig. 1: A waterproofed Bend Sensor installed in a PVC pipe union and interfaced with a voltage divider and analog-to-digital converter chip.

The unique serial number is important for calibration purposes. The following sections demonstrate that calibrating and assigning individual calibration coefficients to each sensor is necessary, and the serial number provides a link between an individual sensor and its calibration data in a central database. The main reason the individual devices have different calibration coefficients is that small changes in resistance characteristics can lead to significant changes in output voltage. Some analysis of the sensor's underlying mechanical properties will help illustrate this point.

The BendSensor's deflection is too large to be properly described by small-deflection beam theory. Alben [4] investigated large deflections of a fiber in a flow of Re 2,000-40,000 experimentally and theoretically, and found that the fiber shape minimizes the sum of elastic energy in the fiber and kinetic energy in the flow. Our Re is in the mid- to high end of this range. At this Re, viscous forces (the tangential drag force exerted by the flow over the surface of the fiber) contribute little compared to the normal inertial force of fluid pushing on the fiber [4]. As the flow velocity increases, the fiber shape becomes quasiparabolic:

$$X = 1.34 Y^{1/2} \qquad (1)$$

where X and Y are related to the fiber's actual spatial coordinates (x,y) scaled by the double fiber length and a dimensionless parameter η:

$$\eta^2 = \frac{4\rho f L^3 v_s^2}{E} \text{ and } X = \frac{x\eta^{2/3}}{2L}, Y = \frac{y\eta^{2/3}}{2L} \qquad (2)$$

This parameter is a function of the flow velocity v_s, the fluid density ρ (1g/cm^3), the fiber's dimensions (here, the length L=40.6 mm and width f=8mm), and the fiber rigidity E – the product of the elastic modulus and beam moment of inertia. In this work, the elastic modulus for the sensor's polyimide substrate was used (2.5 GPa), and the moment of inertia was $t^3f/12$, where the sensor thickness t = 0.2 mm. For comparison with experimental results, the computed η was then divided by 2.8, an empirical factor that accounts for the wake pressure behind the bending fiber [5].

Given the shape in equation (1), and with measurements of the resistance of the BendSensors wrapped around circular mandrels, it is possible to investigate the sensors' resistance-vs-velocity characteristics by integrating the resistance as a function of local radius of curvature. Note that because the sensors start out in the small-deflection regime and approach the parabolic shape for η>>1, with a gradual transition to the parabolic regime around η=5.6, and our η ranges from 10 to 20, the parabolic model will overpredict the curvature (and the corresponding sensor voltage) at the low end of the flow velocity range, and better match the sensors' asymptotic behavior at the high end of the range.

The parabolic shape in (1) can be parametrized in x as:

$$y = \frac{x^2}{2r_o} \qquad (3)$$

where r_o is the radius of curvature at the base of the parabola (x=0), and x and y are the sensor's actual spatial coordinates. The velocity dependence of the BendSensor's shape is now contained within r_o, a single parameter that sets the parabola's shape at a given velocity. At v=0, the sensor will be straight (r_o=∞), while at larger flow velocities the sensor bends and r_o

takes on a smaller value. In equations (4) through (6), we calculate the total resistance as a function of r_o, use a voltage divider construction to determine the resulting sensor voltage, then invert the r_o function to plot sensor voltage as a function of flow velocity for a variety of resistance-vs-radius characteristics measured from different BendSensors.

The local radius of curvature of the parabola described by Equation (3) is a function of the *x*-coordinate:

$$r_{local}(x) = r_o\left(1+\left(\frac{x}{r_o}\right)^2\right) \tag{4}$$

and the local arclength of the parabola as a function of *x* is:

$$ds(x) = \sqrt{1+\left(\frac{dy}{dx}\right)^2} = \sqrt{1+\left(\frac{x}{r_o}\right)^2} \tag{5}$$

The total resistance is

$$R_{total} = \int_0^{x_{end}} R'(r_{local}(x))ds(x) \tag{6}$$

where *R'* is the *local* resistance per unit length, which will be obtained from measurements from BendSensors, and x_{end} is the final *x*-coordinate obtained by integrating the parabola arclength to obtain the total length *l* of the resistive material in the undeflected BendSensor:

$$l = \int_0^{x_{end}} ds(x) \tag{7}$$

Typically *l* is 36.5 mm for the sensors used here. An analytical solution to (7) enables solution for x_{end} as a function of r_o by finding the zero crossing of (8):

$$x_{end}\sqrt{1+\left(\frac{x_{end}}{r_o}\right)^2} + r_o \ln\left(\frac{x_{end}}{r_o} + \sqrt{1+\left(\frac{x_{end}}{r_o}\right)^2}\right) - 2l = 0 \tag{8}$$

To find $R'(r_{local})$ experimentally, the BendSensors were wrapped around circular mandrels of diameters 14 to 200 mm, and the total resistance *R* was measured. Resistance per unit length *R'* was then calculated as *R*/*l*. This quantity is plotted in Fig. 2, which shows two measured BendSensors (Sensors 1 and 2) with different resistance characteristics. Sensor 2 was also shifted by a small constant amount to represent the common situation of a sensor with bending characteristics close to that of sensor 2, but with a slightly different initial resistance. Sensor resistance increases dramatically as the bend radius tends toward zero. An exponential fit captures the data in Fig. 2, and the resulting equations are listed for the three examples in Fig. 2, giving an expression for resistance per unit length *R'* for use in equation (6). The sensors are connected with a fixed 10 kΩ resistor in a voltage divider configuration with a 5 V input voltage, giving sensor output voltage

$$V_{out} = 5V\left(\frac{R_{total}(r_o)}{R_{total}(r_o)+10k\Omega}\right). \tag{9}$$

A plot of V_{out} vs r_o shows an increasing output voltage as r_o decreases, but it is more informative to examine V_{out} vs flow velocity by inverting the r_o equation obtained from equations (1) through (3):

$$v_s = \left(\frac{r_o}{L}\right)^{-1.5} 2.4\sqrt{\frac{E}{4\rho f L^3}} = r_o^{-1.5}\,(\text{constants}) \tag{10}$$

Fig. 3 is a plot of V_{out} vs $\left(\frac{r_o}{L}\right)^{-1.5}$ which is proportional to flow velocity.

Fig. 3 illustrates that even a small variation in Bend Sensor resistance characteristics has a significant impact on the final output voltage across the measurement range, making individual calibration important. Additionally, effects of different bend sensor mechanical properties (elasticity,

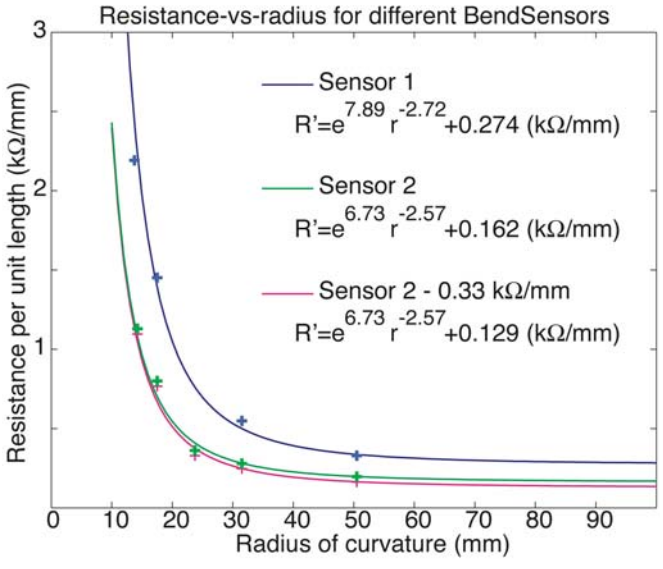

Fig. 2: Measured resistance of different BendSensors as a function of curvature radius, and exponential fits.

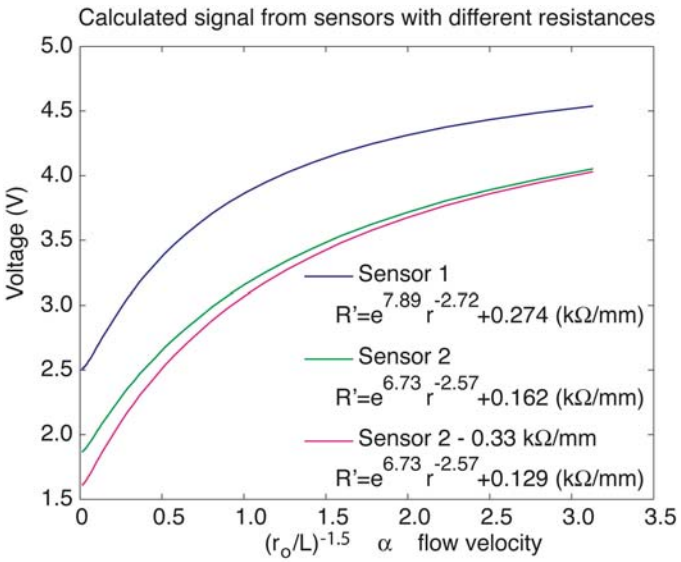

Fig. 3: Calculated voltage signal from the three sensors in Fig. 2 using the parabolic shape model.

thickness, surface roughness) and packaging (length of the flexible seal between the BendSensor resistive element and the sensor interface circuit) will produce variations in the voltage-vs- flow velocity relationship for different sensors. Individual calibration of the fully packaged sensors in a test flume will add greatly to reliability of measurements taken with the system.

IV. High Speed Analog Sensor Tests

To compare the flexible sensors with a standard flow velocity measurement, the sensors were installed in a test flume alongside the ADV sensor. The system used to generate fluid flow in these experiments was a 50-foot long, two-foot wide flume with a variable water flow rate controlled by a pump and valve. The flow sensors were attached to PVC pipes clamped to the top of the flume. The PVC pipes provided mechanical anchoring and also a sealed dry conduit for the voltage divider circuit and wires connecting the ground, signal, and power to the sensors.

For high-speed data acquisition (50 Hz) a LabView interface was used to sample the analog voltage output from three flexible flow sensors. The 50 Hz sampling rate is fast enough to capture ~0.1 second duration peaks and troughs that are observable by ADV. These features are attributed to turbulence in the flume, and their amplitude increases with flow velocity. Fig. 4 shows sample data from both the ADV in Fig. 4(a), and from the three flexible sensors in Fig. 4(d), then compares the noise seen in the ADV sensor with a typical flexible sensor. Both sensor types have noise that drops off with frequency but is otherwise distributed evenly across the spectrum, without any notable peaks at frequencies up to half the 50 Hz sampling frequency. The noise spectrum is shown in Fig. 4(b) for the ADV and Fig. 4(e) for the flexible sensor. The noise originates largely from turbulent velocity fluctuations. Although the flexible sensor has a mechanical resonance in the range of ~10 Hz, an anomalous response is not seen at the resonant frequency due to heavy damping by the surrounding fluid [6].

At a given steady flow velocity, both the ADV and flexible sensors produce a constant output value with relatively large random fluctuations on either side. The amplitude of the fluctuations grows as the flow velocity increases. Fig. 4 (c) shows the distribution of fluctuations above and below the mean value of the ADV signal for a large sample set collected at a flow velocity of 60 cm/s. The fluctuations are tens of cm/s, but the distribution is symmetric, so the precision is greatly improved by averaging dozens or hundreds of successive measurements. Specifications for this type of sensor list a flow velocity uncertainty of 0.5 cm/s.

A similar situation was observed for the velocity signal from the flexible sensors in the analog tests. Fig. 4 (f) shows a symmetric noise distribution for the flexible sensor at two flow velocities, and also for static deflection where the sensor has been removed from the flume. The fluctuation amplitude is larger for the higher flow velocity, and extremely narrow when the sensor is not experiencing turbulent flow. In the last case, the fluctuations were on the scale of the quantization levels of the 12-bit voltage signal ($5V/2^{12}$)=1.2 mV. Analyzing deviations from the mean is a simple process that can be carried out by the processor on a wireless node. A suddenly narrow set of deviations could indicate that a sensor is exposed

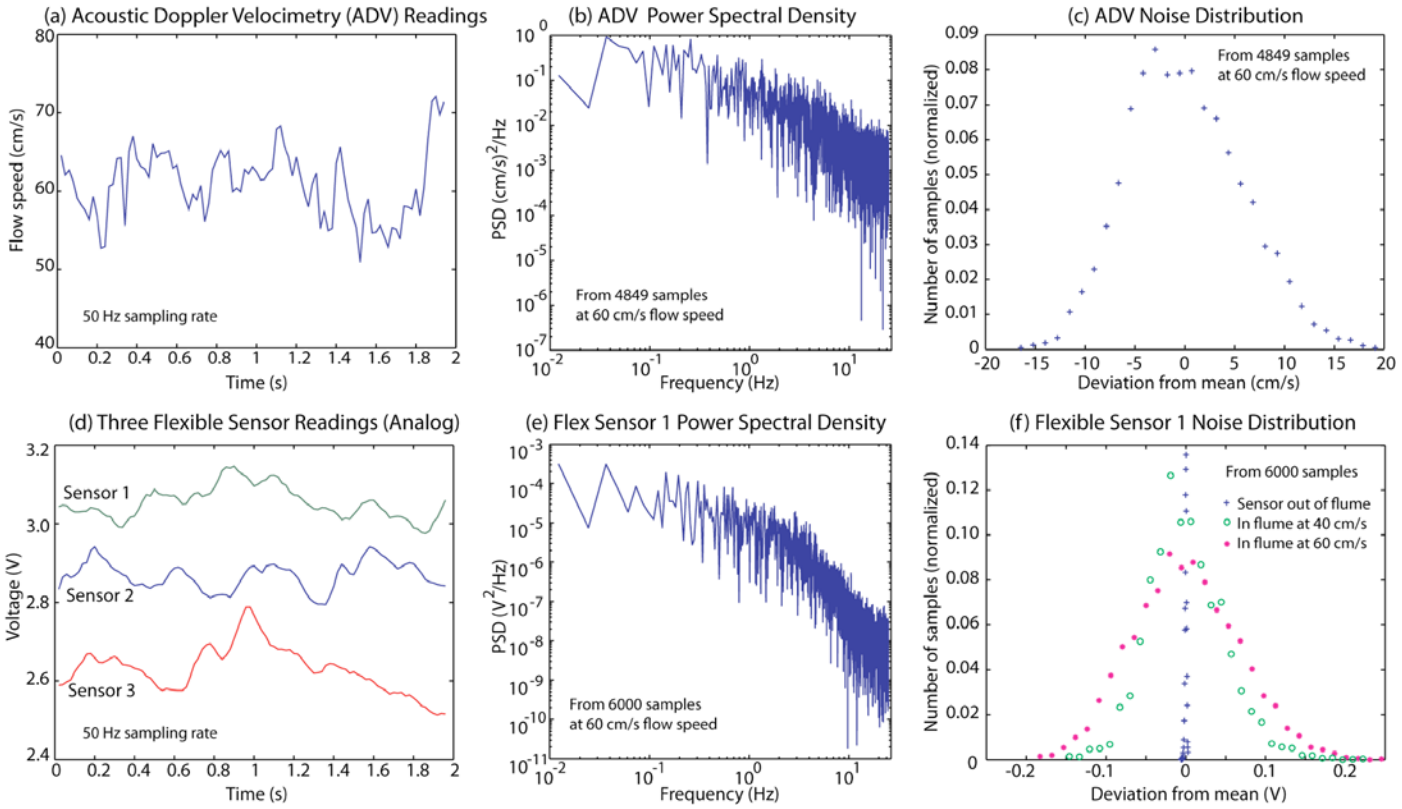

Fig. 4: Comparison of Acoustic Doppler Velocimeter and flexible flow sensors. (a)ADV time series, (b) ADV noise spectrum, (c) ADV fluctuation statistics, (d) time series for three flex sensors, (e) flex sensor noise spectrum, (f) flex sensor fluctuation statistics for two flow velocities and zero static deflection.

above the water line during a drought. Even more interesting, if a flexible sensor becomes jammed into a static position by debris, or covered in sediment, it might still be bent and would indicate flow. However, the small deviations could indicate that the flow data should be disregarded.

During the flume tests, the average sensor voltage output increased with flow velocity as expected due to increased resistance of the bend sensor as it experienced greater deflection. During sensor deployment, the sensors will be switched on at intervals of 1 minute or even greater in order to conserve battery power in the field. It will be important to collect several samples during this sampling time so that the turbulent fluctuations can be averaged out. It is also important to consider the impact of the fluctuations upon sensor calibration. While battery conservation is less important during lab-based use of the wireless sensor network, meaning that it is possible to sample more often than once per minute, the maximum sampling rate of the combined wired/wireless network is approximately 3 Hz per sensor. This means the flume should be kept at a constant volumetric flow rate during collection of several minutes of voltage data from the batch of sensors during calibration. Analysis of the calibration results will enable an estimate of the minimum number of samples required to reach the specified 3% uncertainty at each flow velocity.

V. Mass Calibration via Wireless Sensor Network

For calibration of multiple sensors, the sensors were each interfaced to an onboard A/D chip (the DS2450), which was connected to a wireless sensor node (Crossbow TelosB) programmed to communicate with the DS2450s using the 1-Wire protocol. Voltage data from two sensors on each of six wireless nodes was collected on a PC equipped with another TelosB node programmed as a receiver. In Fig. 5, the installed flow sensors and ADV sensor are visible at the base of the flume before filling. Also onboard each flow sensor was a 1-wire temperature sensor (Maxim DS18B20) for tracking ambient water temperature at the sensor, since temperature affects sensor deflection by thermal expansion of the Bend Sensor and changes fluid viscosity and density. A relatively small temperature dependence of -2 mm/s per C was observed using these sensors.

Several PVC test stands were installed to anchor the sensors and protect circuitry and wires from the water. At the top of each PVC structure, the TelosB wireless node was housed in a plastic water-tight capsule with a 4-AA battery pack. Even when the dielectric capsule was sealed with a threaded lid, the signals could readily travel ~100 feet from the nodes' printed circuit antenna to the data collection computer.

Twelve sensors were calibrated simultaneously by setting the flume at each of nine volumetric flow rates for several minutes, and collecting a data file during that time. Each wireless sensor can address upwards of 100 sensors [7], so the calibration system can potentially handle many more sensors at once. With fewer sensors per node, however, each sensor is sampled more frequently for faster overall calibration.

The incoming sensor data were stored as text files with each data line listing the sensor's serial number, radio node number, and sensor voltage along with packet count and related radio packet information in hexadecimal format. Because individual nodes were switched on at different times, the data from different flow sensors appeared in a random sequence and had to be kept together with the serial number for individual calibration.

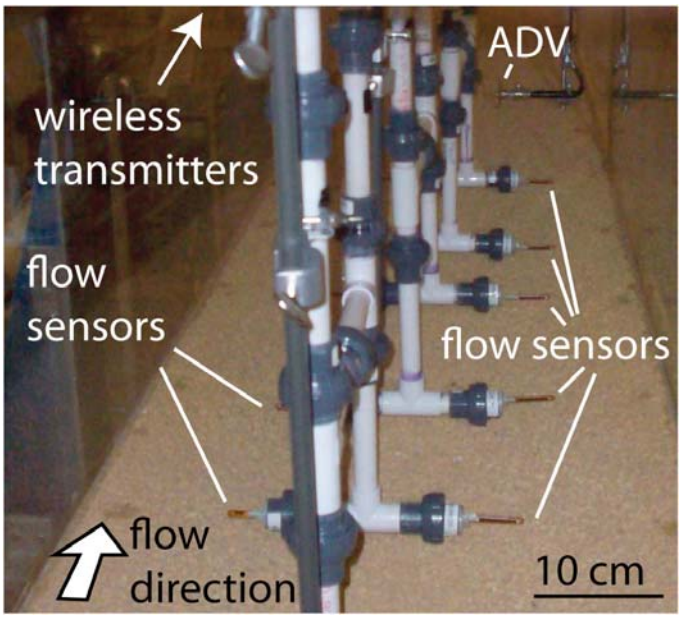

Fig. 5: Flow sensors and Acoustic Doppler Velocimeter (ADV) in test flume.

A Perl script identified the voltage series associated with each sensor, and converted the bytes to decimal values in a comma-delimited text format for data-fitting and visualization in software packages such as MATLAB or Excel. Each sensor reported its voltage 40 to 400 times for each flow velocity, depending upon the length of the test, and these data were averaged to produce points for fitting. A small fraction (<1%) of the values were at the minimum or maximum ends of the voltage range (0V or 5V). These were attributed to faulty data packets and were discarded.

Fig. 6 shows this data for three different flexible sensors over a range of flow velocities from 0.3 m/s to 0.6 m/s. Sensor 05, which did not have the current monitoring circuit that was fitted to Sensors 5D and 08, was observed to have lower noise due to a cleaner supply signal. Fig. 7 shows how the voltage-vs flow velocity data approaches the parabolic model at the high end of the flow velocity range. In order to provide the velocity (x-coordinate) for these plots, local velocity estimates were obtained from experimental measurements and hydraulic modeling at each sensor location. An acoustic Doppler velocimeter (ADV) was used to measure the velocity distribution with depth in the channel, and eleven measurements each with a 50 Hz sampling frequency and 6,000 points were used to calculate the time-average velocity, $\overline{u}$, at each depth. It was found that the velocity profile $\overline{u}(y)$ followed a logarithmic distribution as

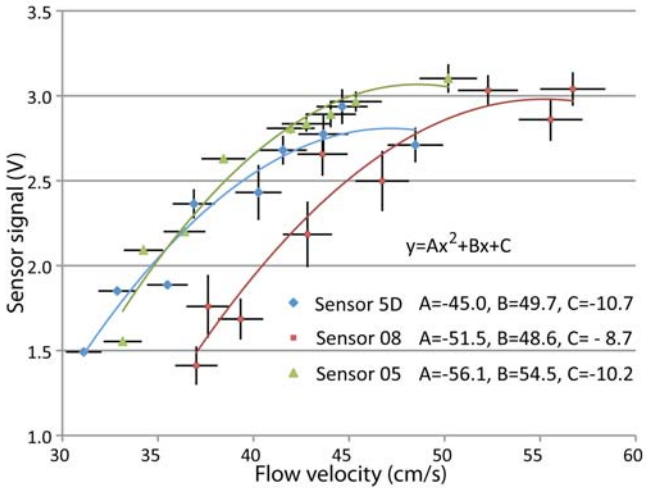

Fig. 6: Flume data and parabolic fits for three different flow sensors.

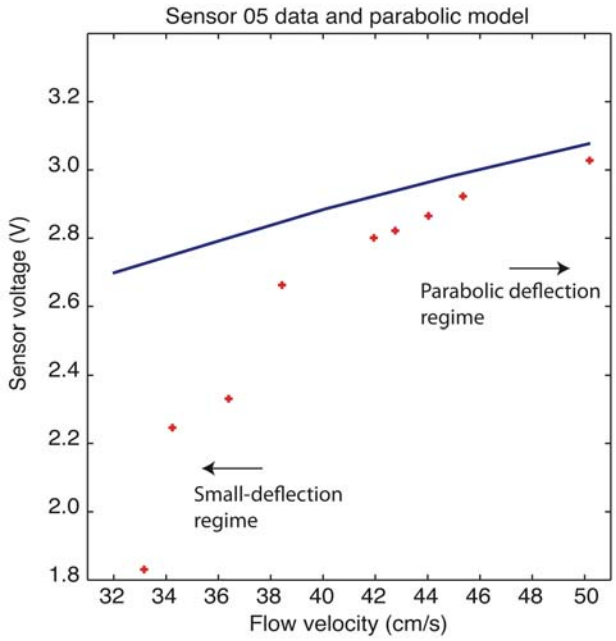

Fig. 7: Solid line: parabolic deflection model (from middle line in Fig. 3) scaled to flow velocity in cm/s. Points: data from Sensor 05. At high velocities, data and model converge in the parabolic deflection regime.

$$\frac{\bar{u}(y)}{u_*} = B_1 + B_2 \ln\left(\frac{y}{k_s}\right) \tag{11}$$

where u_* is the friction velocity and approximated as

$$u_* = \sqrt{gRS} \tag{12}$$

where g is the gravitational constant, R is the hydraulic radius ($R=AP^{-1}$, where A is the area of the channel and P is the wetted perimeter), and S is the energy gradient. In Equation (11), B_1 and B_2 are coefficients and values of 8.5 and 2.5 were found to fit the velocity distribution well, thus agreeing with reported logarithmic distributions for a fully rough turbulent flow [8]. Here k_s is the roughness height and a value of 10 mm was fitted to the data, which agreed well with the D_{max} (the maximum diameter of gravel for the gravel-bed in the flume). Equation (11) was solved for each sensor at the fixed location of y=2.5 cm, where the sensors were placed, however, the flow depth H varied longitudinally throughout the test section due to the placement of the sensors in the flow because of the backwater effect [9] that caused a gradually varied flow profile in the upstream half of the sensors. To account for the backwater effect, S was calculated for each sensor location using continuity ($Q=VA$), followed by integration of Equation (11) to determine the average velocity, and substitution of Equation (12) as

$$S = \left[\frac{Q}{A\sqrt{gR}\left(6 + 2.5\ln\frac{H}{k_s}\right)}\right]^2 \tag{13}$$

where the discharge, Q, in the rectangular channel was measured using a Venturi meter and acoustic Doppler velocity meter that were within the pipeflow delivery system. The measurement and calculation showed less than 3% difference in discharge estimates.

These local flow velocities were used to calibrate the flow sensors in Fig. 6. Over this relatively small range, the sensor voltages increased from 1.5 to 3V. The sensor voltage follows a parabolic trend over this range. Over a larger range, an odd-order polynomial fit better captures the data, as the voltage divider output asymptotically approaches the minimum voltage at zero deflection, and the maximum of 5V at full deflection. A linear fit to this data produced results with different coefficients that depended upon the stiffness and initial electrical resistance of each BendSensor. Therefore, individual calibration coefficients were collected for each sensor.

VI. Field Deployment of Flow Sensors Wirelessly Linked to Data Logger

High spatial resolution, low-cost flow sensors are needed for detailed studies of sediment transport in watersheds. Therefore, an existing sediment research site in Eastern Kentucky, Lilley Cornett Woods, was chosen for outdoor deployment of the flow sensors. The site is remote, without electrical power and impractical to visit more than once per week, so long-term battery powered operation was required. Sensor nodes were tuned for low-power operation on 4-AA battery packs by reducing the sampling rate to ~10 samples per hour, by turning off the radio between data broadcasts, by shutting off all indicator LEDs on the radio boards, and by turning on individual BendSensors only while sampling the flow.

The data logging system then became the lifetime-limiting component. Instead of a computer, a low-power microcontroller-based logger (Logomatic V2 Serial SD Datalogger, Sparkfun Electronics) was connected to the receiver node, a Crossbow TelosB programmed with the default TOSBase receiver program (online repository: http://www.tinyos.net/tinyos-1.x/apps/TOSBase/). The data

connection was made by joining the Logomatic RXIO pin to a wire soldered to pin 34 (UART1 TX) of the MSP430 microcontroller on the TelosB board. The Logomatic was configured to run at 57600 baud, and was powered by a 6V, 14Ah sealed lead acid battery; its onboard 3 V regulator was used to power the TelosB receiver board. The entire data logging system was stored in a waterproof case on the stream bank approximately 15 feet from the wireless flow sensors. No external antenna was necessary to receive the sensor signals.

After powering up, the Logomatic began receiving bytes from the TelosB board and storing them in a binary file in its onboard micro-SD card. Data files were later converted to text for recovery of a time series from each sensor using the previously described procedure, and for sensors 5D and 5C, flume-based calibration coefficients were applied to convert voltages to flow velocities.

Besides the new data logger, other considerations for field work included leak-checking and ruggedizing the sensors. Leak checks were conducted indoors by pumping air into the sensor housings while the sensors were immersed in water. Areas with bubbles were dried and patched with 5-minute epoxy (Loctite). Wire cages around the sensors helped prevent damage during transport, but the cages interfered with the flow pattern by trapping leaves and other debris, so cages were removed for deployment in the watershed. The stream at this point in the watershed was relatively shallow (~10 cm), meaning sensors had to be installed horizontally by attaching to two stakes across the stream, rather than vertically as planned for deeper sections.

Fig. 8 illustrates the sensor installation upstream and downstream of an existing sediment sampler. Flow velocity data will aid analysis of the sediment load from this sampler, and when charted alongside local rainfall data, will indicate how the watershed responds to precipitation. At the bottom of Fig. 8, rainfall data is plotted from a weather station approximately 6 miles from the site (MKY 120, US-119 at Pine Mountain). Corresponding time series of flow velocities from the upstream and downstream sensors show gradually decreasing flow after a storm that occurred the day before installation.

VII. Refinements for Improving Sensor Uncertainty

A more detailed analysis was carried out to estimate the minimum number of voltage measurements needed for the flexible sensors to achieve a 3% uncertainty in the average flow velocity. The voltage-vs-flow velocity relationship was inverted in MATLAB, then fit with a higher-order polynomial. Fig. 9 shows this data and fit for Sensor 05, along with error bars designating the ADV's specified 0.5 cm/s uncertainty. The polynomial fit was then differentiated to calculate the effect of voltage uncertainty ΔV on flow velocity uncertainty Δu:

$$\Delta u = \frac{\partial u}{\partial V}\Delta V \qquad (14)$$

For the voltage uncertainty, the standard deviation σ was computed from at least 40 voltage samples collected at each flow velocity. For a quantity with random fluctuations like

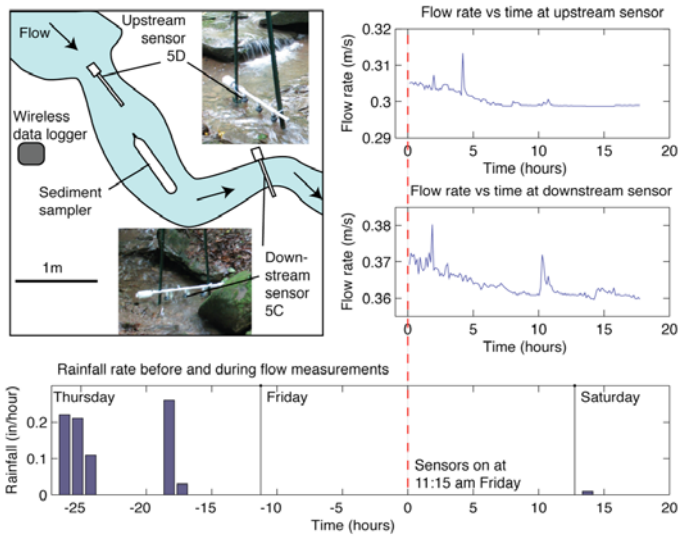

Fig. 8: Flow sensor deployment at Lilley Cornett Woods sediment research site, with data from flow sensors and local rainfall records.

those in Fig. 4(f), the standard deviation of the average of N measurements is $\sigma/\sqrt{N}$:

$$\Delta u = \frac{\partial u}{\partial V}\frac{\sigma}{\sqrt{N}}. \qquad (15)$$

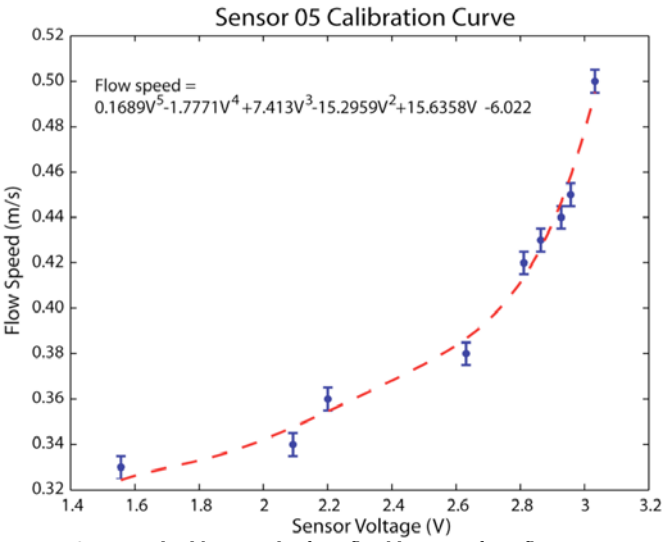

Fig. 9: Inverted calibration plot for a flexible sensor from flume tests. Calibration coefficients were obtained by a least-squares polynomial fit.

Solving equation (2) for N, the maximum required values of N occur at the high end of the flow velocity range. For 3% uncertainty at 0.5 m/s (Δu=1.5 cm/s), 30 or more samples need to be collected and averaged. This means at least a 10-second data acquisition time at 3 Hz. This is acceptable in the environmental sensor application where the flow pattern varies over a long time scale. It should be emphasized that the resulting uncertainty is for the time-averaged flow velocity, rather than the instantaneous flow velocity, which is always subject to turbulent fluctuations for any flow sensor.

For many applications, a higher data rate is desirable at fast flow velocities. The number of required samples increases near the higher end of the flow velocity range not only because the turbulent fluctuations (σ) are larger at higher velocities, but also because the slope (du/dV) of the flow-velocity-vs-voltage curve in Fig. 9 steepens. This is where the bend sensor starts to reach its maximum deflection and the voltage divider its maximum voltage. For this sensor, the turndown ratio (or ratio of maximum to minimum measurable flow rates) is at least 2. The ratio can be extended using a set of flexible sensors having different lengths, mechanical properties and resistance values, so that for the flow velocities of interest, at least one of the sensors is always in the beginning of its deflection curve. An alternative to this multi-sensor approach would use an analog-to-digital system with sensitivity matched to a single sensor's nonlinear velocity-vs-voltage deflection curve [10].

VIII. Conclusions And Future Work

Wireless sensors were chosen over wired sensors for their practical advantages in the field, but they also offered many unanticipated benefits for sensor development and calibration during this project. The wireless data acquisition system made setup and calibration run smoothly, especially for tests where it was desirable to move sensors around in the flume between tests (for instance, determining whether a sensor's position in the flume had a strong effect on the calibration results). The lack of signal and power wires reduced setup time and resulted in fewer errors due to disconnected or shorted wires, even compared to the relatively simple three-sensor LabView setup used for high-speed data collection. Because the sensor nodes were continually broadcasting data throughout the lab, two researchers were able to independently collect a calibration data series on individual laptops equipped with a TelosB receiver mote. This type of redundant data collection may be useful for noisy situations where dropped radio packets are expected, or in sensor laboratory classes where there is one system under test, but several students are interested in gathering and plotting data.

In an application where rapid flow velocity swings are expected, it will be important to consider the relaxation and any hysteresis of the sensor [11]. These sensors took some time (seconds to minutes) to fall back to their original resistance values after being removed from the flows. This is acceptable only if the flow history is known or if a creep compensating sensor is present [12]. The sampling rate must be matched to the experiment so that sudden flow changes do not go unobserved between samplings. Otherwise, a smaller sensor made of a stiffer material could be considered [13,14].

For data visualization, the end user needs a set of spatial coordinates, sensor orientations, and timestamps to go with the sensor data and the calibration coefficients. It is the project goal to automate the spatial data reporting as much as possible. The location problem breaks down into discovering the sensors' position in the plane, and locating each sensor's depth beneath the water. Wireless sensor network locationing is an active field of research, with popular trilateration methods based on time-of-flight of an acoustic signal vs a radio signal, or on the received signal strength of a radio signal from a beacon. However, radio-based methods do not work well under water due to signal attenuation. We take advantage of the existing wiring to find the linear sequence of the sensors on a cable underwater [15], while the above radio methods will work to locate the planar coordinates of the above-water radio nodes.

Sensor spatial orientation remains to be automated. In some cases (temperature, hydrostatic pressure) sensor orientation is relatively unimportant, but for the flow sensor it matters a great deal. A multi-axis flexible sensor might be able to determine its orientation based on the axis that experiences the most deflection.

The calibration setup shown in Fig. 5 was designed to put all sensors at equivalent locations with respect to their distance from the bottom and sides of the flume because these distances determine linear flow velocity at the sensor's position. However, when using the sensors to carry out environmental research, one goal is to measure the total flux of sediment at a point along a stream. This requires sensors to be placed in a vertical grid over a cross-section of the streambed. The sensors were designed with a modular electrical and mechanical interface for easy adaptation to field sites having a wide variety of configurations. Work continues in the area of user configurability, because a major aim of the project is a multiparameter sensor system for education and environmental research that does not need extensive programming by engineers. In the next stage of the project, the wireless platform will be used to test micro and nanomaterial-based devices for chemical sensing [16-18].

Acknowledgments

We thank Nitin Matnani, Evgenia Moiseeva, and Yehya Senousy at the University of Louisville for assistance with mass sensor calibration in the test flume, Darren Martin, John Allison and Nikki Byrd at the University of Kentucky for assistance with outdoor deployment of the sensors, Sarah Courtney at Eastern Kentucky University for flow sensor prototyping, and Alice Jones at Eastern Kentucky University for facilitating the field sampling part of this project.

References

[1] Harnett, C. K., Courtney, S. M., and Kimmer, C. J., "SALAMANDER: A distributed sensor system for aquatic environmental measurements," Proceedings of IEEE International Instrumentation and Measurement Technology Conference, Victoria, BC May 12-17, 2008, p 1787-1792.

[2] Harnett, C. K., Blumenthal, N., Hopf, K. L., Fox, J. F., and Pulugurtha, S., "Wireless sensor network for calibration and deployment of low-cost fluid flow-rate sensors," Proceedings of IEEE International Instrumentation and Measurement Technology Conference, Singapore, May 5-7, 2009.

[3] J. M. Dias Pereira, "Flow Meters: Part 1. Part 18 in a series of tutorials in instrumentation and measurement," IEEE Instrumentation and Measurement Magazine 12 18-26 (2009).

[4] S. Alben, M. Shelley, and J.Zhang, "Drag reduction through self-similar bending of a flexible body," Nature 420 479-481 (2002).

[5] S. Alben, M. Shelley, and J. Zhang, "How flexibility induces streamlining in a two-dimensional flow," Physics of Fluids 16 1694-1713 (2004).

[6] *Signal Conditioning and PC-based Data Acquisition Handbook*, chapter 8, ISBN: 0965678911, IOTech Incorporated,1998.

[7] Maxim Integrated Products Application Note 148, "Guidelines for Reliable 1-Wire Networks." Online: http://pdfserv.maxim-ic.com/en/an/AN148.pdf

[8] Chang, H.H. (1988) Fluvial Processes in River Engineering. Krieger Publishing Company, Malabar, Florida.

[9] Jain, S.C. (2001). Open-Channel Flow. John Wiley & Sons, Inc. New York.

[10] J. M. Dias Pereira, O. Postolache, and P. Silva Girao, "A digitally programmable A/D converter for smart sensors applications," *IEEE Trans. Instrumentation and Measurement* vol. 56, p. 158-163, 2007.

[11] M. Rouff, Z. Lakhdari, and M. Cotsaftis, "Analytical model for the correction of the creep and relaxation of weight sensors," proceedings of Modelling, Identification and Control, Feb. 18-21, 2002, track 350-111.

[12] S. Fahlbusch and S. Fatikow, "Force sensing in microrobotic systems-an overview," Proceedings of IEEE International Conference on Electronics, Circuits and Systems, Lisboa, Portugal, September 7-10, 1998, vol 3, p. 259-262.

[13] Chen, N., Tucker, C., Engel, J. M., Yang, Yingchen, Pandya, S., and Liu, Chang, "Design and characterization of artifical haircell sensor for flow sensing with ultrahigh velocity and angular sensitivity," *J. Micromechanical Systems* vol. 5, p. 999-1014, 2007.

[14] D. A. Czaplewski, B. R. Ilic, M. Zalalutdinov, W. L. Olbricht, A. T. Zehnder, H. G. Craighead, and T. A. Michalske, "A micromechanical flow sensor for microfluidic applications," *J. Microelectromechanical Systems* vol. 13, p. 576-585, 2004.

[15] Harnett, C. K. "Determining the physical sequence of sensors on a serial bus with minimal wiring," *IEEE Sensors Journal* vol. 8, p. 382, 2008.

[16] Harnett, C. K., "Interfacing microfabricated and nanomaterial-based sensors with a modular environmental monitoring system," Proceedings of University Government Industry Micro/Nano Symposium, Louisville, KY July 13-16, 2008, p. 120-122.

[17] Davis, C. E., Ho, C. K., Hughes, R. C., and Thomas, M. L., "Enhanced detection of m-xylene using a preconcentrator with a chemiresistor sensor," *Sens. Act. B-Chem.* vol. 104, p. 207, 2005.

[18] Keynton, R. S., Roussel, T. J., Crain, M. M., Jackson, D. J., Franco, D. B., Naber, J. F., Walsh, K. M., and Baldwin, R. P., "Design and development of microfabricated capillary electrophoresis device with electrochemical detection," *Anal. Chim. Acta* vol. 507, p. 95, 2004.